

# Quench dynamics of superconducting fluctuations and optical conductivity in a disordered system

Yonah Lemonik and Aditi Mitra

Center for Quantum Phenomena, Department of Physics,  
New York University, 726 Broadway, New York, NY, 10003, USA

(Dated: June 13, 2022)

There has been significant interest in the generation of very short-lived superconducting states in solid-state films. Here we consider the role of non-equilibrium superconducting fluctuations in such systems, generated by an interaction quench, considering the limit of large static disorder. In particular, we argue that because of critical slowing down, the regime of the fluctuation dominated *normal state* is more important than might be naively thought. We show how such a state might appear in the optical conductivity, and give the appropriate non-equilibrium generalization of the Azlamazov-Larkin and Maki-Thompson fluctuation corrections to the optical conductivity.

Ultra-fast spectroscopy can not only probe dynamics of an electron system on time scales shorter than the thermalization time [1–3], but may even induce non-equilibrium phase transitions through the pump laser [4–8]. Thus a particular topic of interest is studying the out-of-equilibrium behavior of systems near a critical point. Here we address the dynamics of a thin metallic film where the distance to the superconducting critical point varies rapidly, but the system remains in the normal state. We discuss the impure limit  $T\tau/\hbar \ll 1$ , where  $T$  is the temperature and  $\tau$  the elastic impurity scattering time – the clean limit is discussed elsewhere [9, 10].

We find strong signals in the optical conductivity driven by the interplay of critical slowing down and fluctuation conductivity effects. In particular the fluctuation effects must be understood in an inherently non-equilibrium way. This last point may be seen by comparing time-scales. A naïve scale for fast interacting processes is  $\hbar/T \sim 10^{-2}$ ps at room temperature. Thus, if a transient state exists for picoseconds [4], many interactions will occur over the life of the state, perhaps implying some sort of effective equilibrium.

However, there is a much slower scale near criticality: the lifetime of superconducting fluctuations, given by  $\sim \hbar/T\epsilon$ , where the detuning  $\epsilon \equiv (T - T_c)/T$ ,  $T_c(U)$  being the critical temperature for an interaction strength  $U$ . Thus for reasonable trajectories of  $\epsilon(t)$ , see Fig. 1, the fluctuations will relax slower than  $\epsilon(t)$  changes, and will not be describable by an adiabatic approximation. As we will show, we may have  $T < T_c(U)$  for a period  $t \sim (T_c - T)^{-1} \log E_F \tau$  [11], where  $E_F$  is the Fermi energy, without actually undergoing the superconducting phase transition. For  $T_c = 100$ K,  $T_c - T = 5$ K, and  $E_F \tau/\hbar = 100$ ,  $t \sim 1$ ps. Thus a short lived experiment may never detect true superconductivity even though  $T < T_c$ .

The development of large superconducting fluctuations may be detected by measuring the conductivity. The equilibrium theory of fluctuation superconductivity [12] describes how the conductivity is corrected when  $\epsilon \ll 1$ . In this region the electron-electron interactions are dominated by large superconducting fluctuations, even though

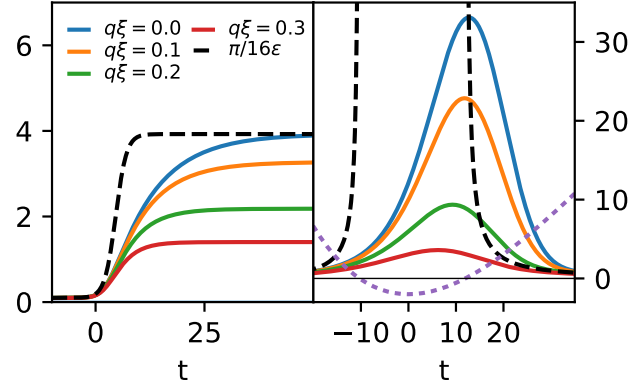


FIG. 1. The growth of the superconducting fluctuation at different lengths ( $q^{-1}$ ) under a changing detuning  $\epsilon(t)$  from the superconducting critical point. The time is given in units of  $\pi\hbar/8T$ . The dashed line shows  $\pi/16\epsilon(t)$  which equals  $B(q = 0)$  in equilibrium. The dotted purple line in the right panel gives  $\epsilon(t)$  at arbitrary scale. In the left panel the detuning saturates at the value  $\epsilon = 0.05$ . In the right panel, the detuning is  $\epsilon(t) = \epsilon_0 + (\epsilon_{\min} - \epsilon_0)(t/t_*e) \exp(-t/t_*)\theta(t)$  with the parameters  $t_* = 30$ ,  $\epsilon_0 = 1$ ,  $\epsilon_{\min} = -0.05$ .

there is no long range superconducting order. This affects the conductivity through three channels. The first is the density of states effect, where incoherent scattering off of the superconducting fluctuations renormalizes the single-electron propagation. In a dirty superconductor this is the weakest effect and negligible. The second effect is the Azlamazov-Larkin (AL) effect [13, 14] where the charged fluctuations serve as an additional channel carrying current. This gives a positive contribution to the conductivity which, in equilibrium, goes as  $\epsilon^{-1}$  in dimension  $d = 2$ .

The third effect is the Maki-Thompson (MT) effect [15–17]. Here an electron diffuses along a random trajectory until it Andreev reflects off a fluctuation. The resulting hole then diffuses through the same random trajectory in reverse. As the electron and hole have opposite

energy, the phase accumulated on the two random trajectories cancel. Thus all trajectories that contribute to this process sum without destructive interference. The only limit on the number of contributing trajectories along which the electron diffuses is inelastic collisions that destroy the phase coherence between the electron and hole trajectory. The time for such processes, the coherence time  $\tau_\phi$ , is not controlled directly by the fluctuations and may be very long,  $T\tau_\phi/\hbar \gg 1$ .

We extend these results to the case of a non-equilibrium  $\epsilon(t)$  caused by a time varying electron-electron interaction. The conductivity correction cannot be obtained by taking the equilibrium calculation with time varying  $\epsilon(t)$ , for two reasons. Firstly, as discussed, critical slowing down means that the size of the fluctuations at time  $t$  is not given by  $\epsilon(t)$ . Secondly, the AL and MT effects are long-lived processes, meaning that they occur on the scale of  $1/T\epsilon$  and  $\tau_\phi$  respectively. As  $\epsilon(t)$  is changing on these time scales, it is not even clear at what time  $\epsilon(t)$  or the fluctuation density should be evaluated. Finally we note that the actual experimentally measured quantity is a convolution of these various time-dependent quantities against the probe electric field signal. Our calculation takes all of these into account.

Our results rest on several assumptions. (i) Self interaction of the fluctuations are neglected, this is valid as long the fluctuations are not extremely large. (ii) The electron occupation numbers relax to a thermal distribution on a time-scale much shorter than the fluctuation lifetime. (iii) The time dependent perturbation, e.g. the driving laser, may be modeled by a time varying electron-electron interaction. (iv) This interaction is smoothly varying on the scale  $\hbar/T$ .

The calculation proceeds by evaluating the appropriate diagrams in the Keldysh technique summarized in Fig. 2, employing the standard diagrammatic technique reviewed in Ref. [18]. The Hamiltonian is

$$H = \sum_{kk's} \left[ (\varepsilon_k \delta_{kk'} + V_{k-k'}) c_{ks}^\dagger c_{k's} + U(t) \sum_{qs'} c_{ks}^\dagger c_{k-q} c_{k'-q} c_{k's'} \right]. \quad (1)$$

Here  $c_{ks}, c_{ks}^\dagger$  are the electron creation and annihilation operators of electrons with momentum  $k$  and spin  $s$ ,  $\nu$  is the density of states, and  $U(t)$  is the time dependent interaction constant. The potential  $V$  is a Gaussian random potential with moment  $\langle V_q V_{-q'} \rangle = \delta_{qq'}/2\pi\nu\tau$ . The conductivity is given by the Kubo formula  $\sigma(t, t') = i \int_{-\infty}^{t'} ds \langle [J(t), J(s)] \rangle$  where the current operator is  $J = \sum_k \frac{\partial \varepsilon_k}{\partial k} c_k^\dagger c_k$ , and  $\langle \cdot \rangle$  signifies both quantum and impurity averaging. Since the system is not time translationally invariant  $\sigma$  depends on both  $t'$  and  $t$  separately.

This calculation may appear very difficult given the underlying time dependence. However the problem

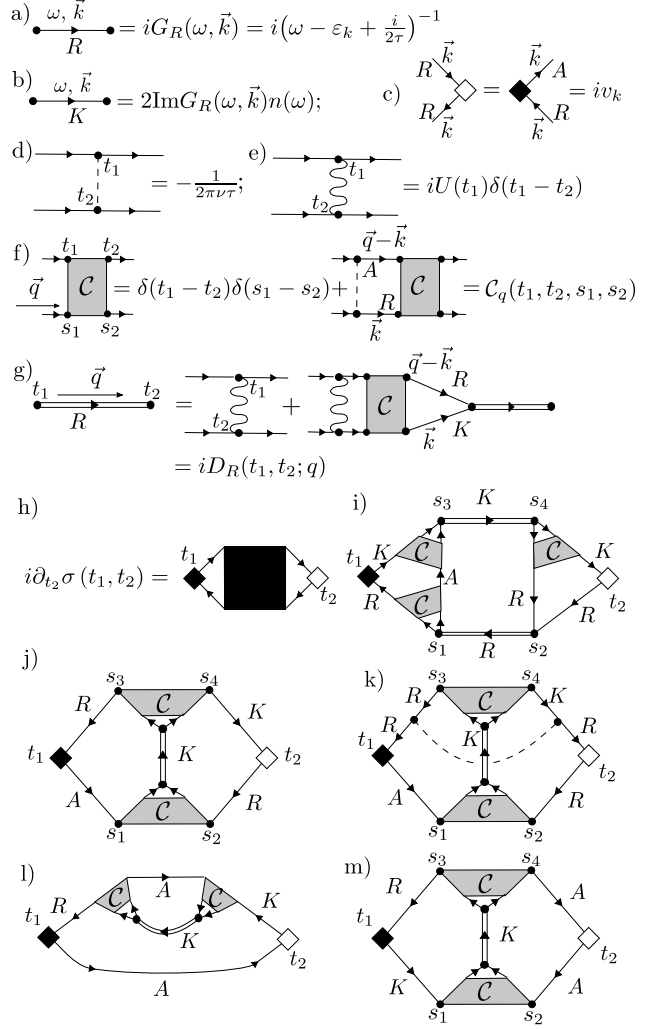


FIG. 2. Elements of the diagrammatic technique. a) Retarded electron Green's function, including finite lifetime due to impurity scattering. b) Keldysh electron Green's function,  $n(\omega) = \tanh \omega/2T$ . c) Current vertices. d) Impurity scattering vertex. e) Electron-electron interaction vertex. The strength of the interaction is allowed to depend on time. f) Cooperon impurity ladder. g) Retarded fluctuation propagator. The Keldysh fluctuation propagator, not pictured, is constructed analogously. h) Kubo formula expansion for the conductivity. The black square represents the sum over all possible diagrams. i) A diagram of AL type. j,k) Two diagrams of anomalous MT type. l,m) Two subleading diagrams: l) a density of states correction and m) a regular MT correction.

is greatly simplified by the existence of two sets of timescales. The first are the "fast" time scales given by  $\tau, T^{-1}$ . These are much shorter than the second set of "slow" time scales given by  $\hbar/T\epsilon(t) = \hbar/[T-T_c(t)]^{-1}$  and  $\tau_\phi$ . As the primary dynamics we are interested in are controlled by the long time scales, functions which are supported only on short time scales may be e.g. expanded in derivatives,  $f(t, t') \approx f_0(t)\delta(t - t') + f_1(t)\partial_t\delta(t - t')$

etc...

In the regime of a good metal  $E_F\tau \gg 1$ , we may neglect all diagrams with crossing impurity lines giving the usual metallic Green's function,

$$G_R(\omega, k) = \left( \omega - \varepsilon_k + \frac{i}{2\tau} \right)^{-1} \quad (2)$$

$$G_K(\omega, k) = [G_R(\omega, k) - G_A(\omega, k)] \tanh \frac{\omega}{2T} \quad (3)$$

where we are taking the electron distribution function  $G_K$  to be its equilibrium value at fixed temperature, the rationale being that the fermion distribution thermalizes on femto-second time scales, while the conductivity is strongly affected by the superconducting fluctuations which thermalize on much longer time-scales. We note in passing that including heating effects via a time-varying temperature is straightforward, as  $G_K(t, t')$  is only supported when  $t' - t \sim T^{-1}$ .

The other significant diagram is the Cooperon  $\mathbb{C}_q(t_1, t_2; s_1, s_2)$ , given in Fig. 2(f). This represents the aforementioned set of processes where in the time  $t_1$  to  $t_2$  an electron diffuses along a random trajectory and a hole diffuses on the same trajectory in reverse in the time  $s_2$  to  $s_1$ .

The Cooperon obeys the equation

$$\begin{aligned} \mathbb{C}_q(t_1, t_2; s_1, s_2) &= \delta(t_1 - t_2)\delta(s_1 - s_2) \\ &+ \int dt' ds' \mathcal{P}_q(t_1, t'; s_1, s') \mathbb{C}_q(t', t_2; s', s_2) \end{aligned} \quad (4)$$

$$\mathcal{P}_q(t, t'; s, s') = \frac{1}{2\pi\nu\tau} \sum_k G_R(t, t'; -k + q) G_A(s, s'; k) \quad (5)$$

In the limit  $t - t', s - s' \gg \tau, T^{-1}$ ,  $\mathbb{C}$  may be written in the form

$$\begin{aligned} \mathbb{C}_q(t_1, t_2, s_1, s_2) &\approx e^{-(t_1 - t_2)\left(\frac{1}{\tau_\phi} + Dq^2\right)} \theta(t_1 - t_2) \\ &\times \delta(t_1 - t_2 + s_1 - s_2). \end{aligned} \quad (6)$$

Here  $D = v_F^2\tau/d$  is the diffusion constant, and  $\tau_\phi$  is take as a phenomenological constant.

We now consider the superconducting fluctuation propagator. It is sufficient to consider only the ladder diagrams, Fig. 2 and neglecting any of the self-interaction of the fluctuations. This is sufficient as long the fluctuations are not "too large" - the precise criterion is given below. We consider the object  $\Pi_R$  multiplying  $D_R$  on the right-hand side of Fig. 2(g),

$$\begin{aligned} \Pi_R(u_1, u_2; q) &\equiv \sum_k \int dt' ds' \mathbb{C}_q(u_1, t'; u_2, s') \\ &\times G_R(t', u_2; k) G_K(s', u_2; q - k) \end{aligned} \quad (7)$$

This is exponentially suppressed unless  $t - t' \lesssim T^{-1}$ . As the system is time translation invariant on this scale we

Fourier transform and use the standard result,

$$\Pi_R(\omega, q)/\nu = \chi(T) + i\frac{\pi\omega}{8T} + \xi^2 q^2, \quad (8)$$

where the coherence length  $\xi = \sqrt{\pi D/8T}$  in the dirty limit, and  $\chi(T)$  is a constant  $\propto \log T/E_F$ . This leads to the following equation of motion for the retarded propagator  $D_R$ ,

$$\left[ \frac{\pi}{8T} \frac{\partial}{\partial t} + \epsilon(t) + \xi^2 q^2 \right] D_R(q, t, t') = \frac{1}{\nu} \delta(t - t'), \quad (9)$$

where the time dependent detuning is related to the interaction by  $\epsilon(t) \approx \frac{1}{\nu U(t)} - \chi(T)$ .

Similarly one may derive that the Keldysh part of the fluctuation propagator  $D_K(t, t') = D_K(t', t)$  can be written as  $D_K(t > t') = \frac{\pi i}{8} D_R(t, t') B_q(t')$ . Here we have introduced the dimensionless fluctuation density  $B_q$ , which obeys the differential equation:

$$\left[ \frac{\partial}{\partial t} + \frac{16T}{\pi} (\epsilon(t) + \xi^2 q^2) \right] B_q(t) = T. \quad (10)$$

We may now precisely state the condition for neglecting the self interactions. It is  $B_q \ll E_F\tau$ , which reduces to the usual Ginzburg-Levanyuk [19] criterion in equilibrium. We relegate the derivation to [11].

This gives a sufficient description of the dynamics of the fluctuations. We now calculate the corrections to  $\sigma(t, t')$  caused by these fluctuations. This is the sum of diagrams indicated schematically by the sum of all diagrams of the form 2(h). Some representative diagrams are shown in Fig. 2(i-m), see [11] for further details.

The diagrams are chosen analogously to the equilibrium calculation. First, as we are interested in the effect of large fluctuations, we include only diagrams containing  $D_K$ . As  $D_K \sim B_q$  grows with small  $\epsilon(t)$  this is sufficient to produce a singular correction. However this effect alone is somewhat weak. For example, in equilibrium  $B_q \propto (\xi^2 q^2 + \epsilon)^{-1}$  and integrating over  $d^2q$  gives only  $\log \epsilon$ .

Certain diagrams have an additional enhancement. This comes from the fact that the Cooperon and fluctuation propagator are long lived, so that the correction to the conductivity does not vanish for  $|t_1 - t_2| \gg T^{-1}, \tau$  but rather is supported up to the long time scales  $\tau_\phi, 1/T\epsilon(t)$ . This may be seen in Fig. 2(i) where  $t_1$  and  $t_2$  are connected only by long lived fluctuation lines. Similarly, in the anomalous MT contribution Fig. 2(j,k), the slow decay of the Cooperon with time means that  $t_1 - t_2$  may be large. Thus when the low-frequency conductivity is calculated there is an additional enhancement from integrating over  $|t_1 - t_2| \gg \tau, T^{-1}$ . Thus in equilibrium these diagrams diverge as  $1/\epsilon$  as  $\epsilon \rightarrow 0$ .

In the density of states contributions, Fig. 2(l), and the regular MT corrections, Fig. 2(m), this long-livedness is absent and hence they are negligible compared to the

larger AL and anomalous MT contribution. At intermediate impurity concentration  $T\tau \sim 1$  these diagrams become comparable to the MT correction [20]. This will be discussed elsewhere.

Therefore the contributing diagrams are those of the form Fig. 2(i,j,k). These are equivalent to the most divergent equilibrium diagrams, excepting some superficial differences owing to Keldysh technique, *e.g* diagrams (k) and (j) are represented in one diagram in the Matsubara technique.

Evaluating the diagrams analogously to earlier calculations, we obtain for the AL and anomalous MT diagrams,

$$\sigma^{AL}(t_1, t_2) = 32 \int_{-\infty}^{t_2} ds \int \frac{d^2 q}{(2\pi)^2} \xi^4 q^2 \nu^2 |D_R(q, t_1, s)|^2 B_q(s) \quad (11a)$$

$$\sigma^{MT}(t_1, t_2) = 16 D \int \frac{d^2 q}{(2\pi)^2} B_q \left( \frac{t_1 + t_2}{2} \right) e^{-2\left(\frac{1}{\tau_\phi} + Dq^2\right)(t_1 - t_2)} \quad (11b)$$

It may be checked that these expressions reduce to the known results in equilibrium [11].

We note that  $\sigma^{MT}(t_1, t_2)$  has the peculiar property that the fluctuations are evaluated not at  $t_1$  or  $t_2$  but the average time  $(t_1 + t_2)/2$ . Physically, the electron must be excited, diffuse, Andreev reflect, diffuse back and be absorbed. As the two diffusions must be identical, the fluctuations are interacted with precisely halfway in time between the excitation and measurement.

We now consider the appearance of  $\sigma$  for certain choices of  $\epsilon(t)$ . A particularly interesting choice is the critical quench, where  $\epsilon(t)$  switches instantaneously from  $\epsilon(t) = \epsilon_i \geq 1$  for  $t < 0$  to  $\epsilon(t) = 0$  for  $t > 0$ . Substituting for the above expressions in this case we have,

$$\sigma(t_1, t_2) = \frac{2T}{\pi} \left[ -\frac{t_2}{t_1} - \log \left( 1 - \frac{t_2}{t_1} \right) + e^{-2(t_1 - t_2)/\tau_\phi} \log \left( 1 + \frac{1}{2} \frac{t_1 + t_2}{t_1 - t_2} \right) \right], \quad (12)$$

valid when  $T(t_1 - t_2) \gg 1$ . When either  $t_1 - t_2 \gg \tau_\phi$  or  $t_1 - t_2 \ll \tau_\phi$  this becomes solely a function of  $t_2/t_1$ . The scaling behavior is a consequence of the "criticality" of the quench when  $\epsilon = 0$ , and the only "slow" scale is  $\tau_\phi$ .

We now consider how the change in conductivity  $\sigma^{AL} + \sigma^{MT}$  would appear in measurement. For simplicity we plot a time dependent optical conductivity given by  $\sigma(\omega, t) = \int d\tau e^{i\omega\tau} \sigma(t + \tau, t)$ . This is shown for the two quenches in Figs. 3 and 4. (A different, experimentally motivated definition [21] of  $\sigma(\omega, t)$  is considered in [11].)

Fig. 3 displays  $\sigma(\omega, t_0)$  for the quench profile of Fig. 1, left panel. The long time equilibrium result (dashed) has the  $\text{Re}\sigma(\omega)$  increasing as  $\omega \rightarrow 0$  until the slowest

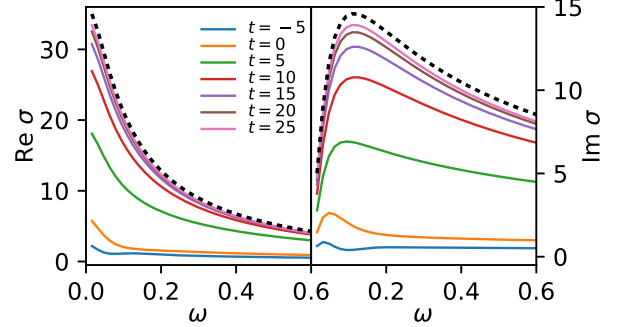


FIG. 3. Conductivity [ $e^2/\hbar$ ] as a function of frequency for several times. The left panel shows real part, the right panel shows the imaginary part. All times are in units of  $\pi\hbar/8T$ . The detuning  $\epsilon$  varies according to Fig. 1, left panel and  $\tau_\phi = 20 \times (\hbar\pi/8T)$ . The dashed line gives the equilibrium result for the final value of the detuning  $\epsilon = .05$ .

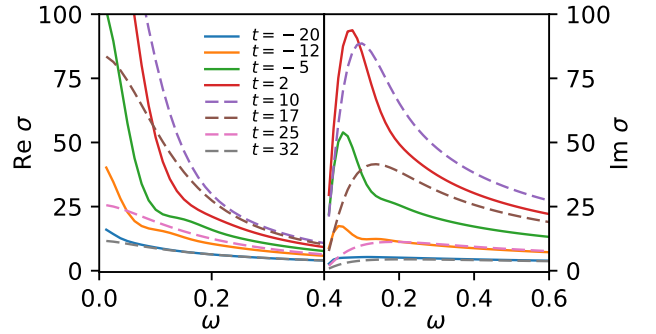


FIG. 4. Conductivity [ $e^2/\hbar$ ] as a function of frequency for several times, all in units of  $\pi\hbar/8T$ . The detuning is given in Fig. 1, right panel and  $\tau_\phi = 20 \times (\hbar\pi/8T)$ . In order to improve clarity, lines for  $t \leq 2$  are shown with full lines and those for  $t > 2$  are shown with dashed lines. The conductivity  $\sigma$  as  $\omega \rightarrow 0$  reaches a maximum of  $\sim 175$  at  $t \approx 7$ .

frequency  $\min(\tau_\phi^{-1}, \epsilon T)/\hbar$  is reached. Below this frequency, the curve flattens to its DC value. Correspondingly there is a peak in  $\text{Im}\sigma$  at this same slowest frequency. In the time dependent results (full lines) we may directly see critical slowing down and thermalization. The conductivity converges to its equilibrium value but only on a slow time scale  $\approx 20 \times (8T/\pi)$ , significantly wider than the underlying quench. Fig. 4 shows  $\sigma(\omega, t_0)$  for a quench profile more appropriate to a solid state system, where a pump laser smoothly changes the interaction with time. In particular we give the case where instantaneously  $\epsilon(t) < 0$  but the size of fluctuation may remain within the  $B_q \ll E_F\tau$  limit. Although the conductivity increases and decreases as expected (i) the peak of the conductivity lags the minimum of the detuning, (ii) the actual dependence of  $\sigma(\omega)$  on  $\omega$  is not given by any equilibrium choice of parameters. Indeed the profiles of the conductivity on the ramp-up are markedly different

than on the ramp down. This is not surprising as the corrections are determined by the fluctuations, and the fluctuations are determined by Eq. (10) - and not any equilibrium distribution. The peak of the low frequency  $\text{Re}\sigma(\omega \rightarrow 0)$  is  $\sigma \sim 175e^2/\hbar$ . This agrees in order of magnitude with the following estimate: setting an effective detuning by the relationship  $\epsilon_{\text{eff}} \equiv \pi/16B(q=0)$  and using the equilibrium formula [11] with  $\epsilon_{\text{eff}}$ . For the present quench with  $\max B \approx 35$ ,  $\epsilon_{\text{eff}} \approx 5 \times 10^{-3}$  and  $\text{Re}\sigma(\omega \rightarrow 0) \approx 60$ .

There are several points raised by this calculation. The first is whether the experimental studies of transient superconductivity [4] can be mapped onto this framework. This would both confirm the superconducting nature of the transient state and provide data on the underlying trajectory of  $\epsilon(t)$  and hence of the light-induced interaction. If possible, this allows the direct study of the critical superconducting dynamics, rather than indirectly via *e.g.* Kibble-Zurek effects [22]. It should also be emphasized that the MT and AL effects, which have similar footprints in DC measurements ( $\sim 1/\epsilon(t)$ ) behave fundamentally differently in a time-resolved situation. As the two contributions are differently sensitive to *e.g.* pairing symmetry, time-resolved fluctuation measurements might be capable of elucidating the underlying superconducting order.

**Acknowledgements:** This work was supported by the US National Science Foundation Grant NSF-DMR 1607059.

---

[1] D. Fausti, R. I. Tobey, N. Dean, S. Kaiser, A. Dienst, M. C. Hoffmann, S. Pyon, T. Takayama, H. Takagi, and A. Cavalleri, *Science* **331**, 189 (2011).

[2] C. L. Smallwood, W. Zhang, T. L. Miller, C. Jozwiak, H. Eisaki, D.-H. Lee, and A. Lanzara, *Phys. Rev. B* **89**, 115126 (2014).

[3] J. Zhang, X. Tan, M. Liu, S. W. Teitelbaum, K. W. Post, F. Jin, K. A. Nelson, D. N. Basov, W. Wu, and R. D. Averitt, *Nature Physics* **15**, 956 (2016).

[4] M. Mitrano, A. Cantaluppi, D. Nicoletti, S. Kaiser, A. Perucchi, S. Lupi, P. D. Pietro, D. Pontiroli, M. Riccò, S. R. Clark, D. Jaksch, and A. Cavalleri, *Nature* **530**, 461 (2016).

[5] M. Knap, M. Babadi, G. Refael, I. Martin, and E. Demler, *Phys. Rev. B* **94**, 214504 (2016).

[6] D. M. Kennes, E. Y. Wilner, D. R. Reichman, and A. J. Millis, *Nature Physics* **13**, 479 (2017).

[7] M. A. Sentef, A. Tokuno, A. Georges, and C. Kollath, *Phys. Rev. Lett.* **118**, 087002 (2017).

[8] M. A. Sentef, *Phys. Rev. B* **95**, 205111 (2017).

[9] Y. Lemonik and A. Mitra, *Phys. Rev. B* **96**, 104506 (2017).

[10] Y. Lemonik and A. Mitra, arXiv:1711.10023 (unpublished).

[11] See Supplemental Material.

[12] A. I. Larkin and A. A. Varlamov, in *Handbook on Superconductivity: Conventional and Unconventional Superconductors*, edited by K.-H. Bennemann and J. Ketterson (Springer, 2002).

[13] L. G. Azlamazov and A. I. Larkin, *Soviet Solid State* **10** (1968).

[14] L. G. Azlamazov and A. I. Larkin, *Phys. Letters* **26A** (1968).

[15] K. Maki, *Progress of Theoretical Physics* **40**, 193 (1968).

[16] K. Maki, *Progress of Theoretical Physics* **39**, 897 (1968).

[17] R. S. Thompson, *Phys. Rev. B* **1**, 327 (1970).

[18] A. Kamenev, *Field Theory of Non-Equilibrium Systems* (Cambridge University Press, 2011).

[19] A. P. Levanyuk, *Zh. Exp. & Teor. Fiz.* **36** (1959).

[20] D. V. Livanov, G. Savona, and A. A. Varlamov, *Phys. Rev. B* **62**, 8675 (2000).

[21] D. M. Kennes, E. Y. Wilner, D. R. Reichman, and A. J. Millis, *Phys. Rev. B* **96**, 054506 (2017).

[22] A. del Campo and W. H. Zurek, *International Journal of Modern Physics A* **29**, 1430018 (2014).

## Supplemental Material

A. Nonequilibrium Ginzburg-Levanyuk Criterion .....	6
B. Equivalence to equilibrium .....	8
C. Experimental definition of $\sigma(\omega)$ .....	9

### A: Nonequilibrium Ginzburg-Levanyuk condition

We discuss the selection of the diagrams and the region of applicability. In equilibrium one may derive the appropriate condition by comparing *e.g.* the fluctuation correction to the specific heat with the jump in the specific heat at the critical point (Larkin and Varlamov, arxiv:0109177). Alternatively one may compare the DC correction to the conductivity with the Drude form. Both these lead to the Ginzburg-Levanyuk criterion  $\epsilon \gg 1/E_F\tau$ . This is not satisfactory in our strongly non-equilibrium setting where  $\epsilon(t)$  is not directly connected to the size of the fluctuations, and where there is no single notion of a DC conductivity. Instead we must express the criterion directly in terms of the fluctuation strength.

To do this we note that every diagram in the notation of Fig. 2 may be decomposed in two parts: Fluctuation propagators and closed fermion loops, (possibly containing current vertex insertions). We have seen that fluctuation propagators are of size at most  $D_K(q) \sim B_q T/\nu$  and  $D_R \sim T/\nu$ . (Going forward we suppress the  $q$  subscript as it is expected that  $B_q$  is largest at  $q = 0$ ). Since  $B \gg 1$  we would like to have all propagators be of Keldysh type. However, this is not allowed by causality and we must have at least one retarded fluctuation line per vertex. Thus we may imagine that all lines are of Keldysh type, and then divide by  $B$  for each vertex.

For fermion loops, following our earlier discussion, these may be treated as "short-ranged objects" where all times are separated on the scale of at most  $\hbar/T$ . Thus it may be treated as a delta-function. For example the fermion loop of Fig. 5(a) may be estimated as

$$\Gamma(t_1, t_2, t_3, t_4) \sim \frac{\nu}{T^2} \delta(t_1 - t_2) \delta(t_2 - t_3) \delta(t_3 - t_4). \quad (13)$$

Above we have used that a fermion loop involves a momentum integral which gives a factor of the density of states  $\nu$ . The coefficient then follows on dimensional grounds  $\frac{\nu}{T^2}$  and the fact that  $T\tau \ll 1$ . Similarly we expect a fermion loop with  $n$  vertex insertions to be a delta function times  $\nu T^{2-n}$ .

Since every fluctuation ends in two vertices, we assign the overall factor  $BT/\nu$  for the fluctuation lines as a factor of  $(BT/\nu)^{1/2}$  for each vertex. Further each fluctuation line brings an integral of momentum  $\int d^2q$  which can be estimated as  $\xi^{-2}$ , and every fermion loop impose conservation of momentum in the outgoing fluctuation. This should similarly be estimated as  $\xi^2$ . Combining all of these estimates we have that the fermion loop with  $n$  fluctuation vertices should be estimated as

$$\begin{aligned} \Gamma^n &\sim \left( \frac{BT}{\xi^2 \nu} \right)^{n/2} \left( \frac{\nu}{T^{n-2}} \right) \frac{\xi^2}{B} \\ &\sim T \left( \frac{B}{\xi^2 \nu T} \right)^{n/2-1}, \end{aligned} \quad (14)$$

times the appropriate delta functions. Thus we may neglect diagrams with more than 2 fluctuation vertices in a fermion loop if the quantity  $B/(\xi^2 \nu T)$  is small. Using the fact that  $\xi^2 \sim v_F^2 \tau / T$ ,  $\nu \sim p_F/v_F$ , we see that this gives the criterion  $B/E_F\tau \ll 1$

For concreteness we consider the correction to  $\Pi_R$  given by Fig 5. This is a diagram of type  $\Gamma^{(4)}$  with two outgoing fluctuation lines connected, so we may estimate it similarly as

$$\begin{aligned} \frac{1}{\nu} \delta \Pi_R &\sim \frac{1}{\nu} \frac{\nu}{T^2} \int \frac{d^2q}{(2\pi)^2} D_K(t, t; q) \\ &\sim \frac{1}{\nu T \xi^2} \int dx x B(t, x/\xi), \end{aligned} \quad (15)$$

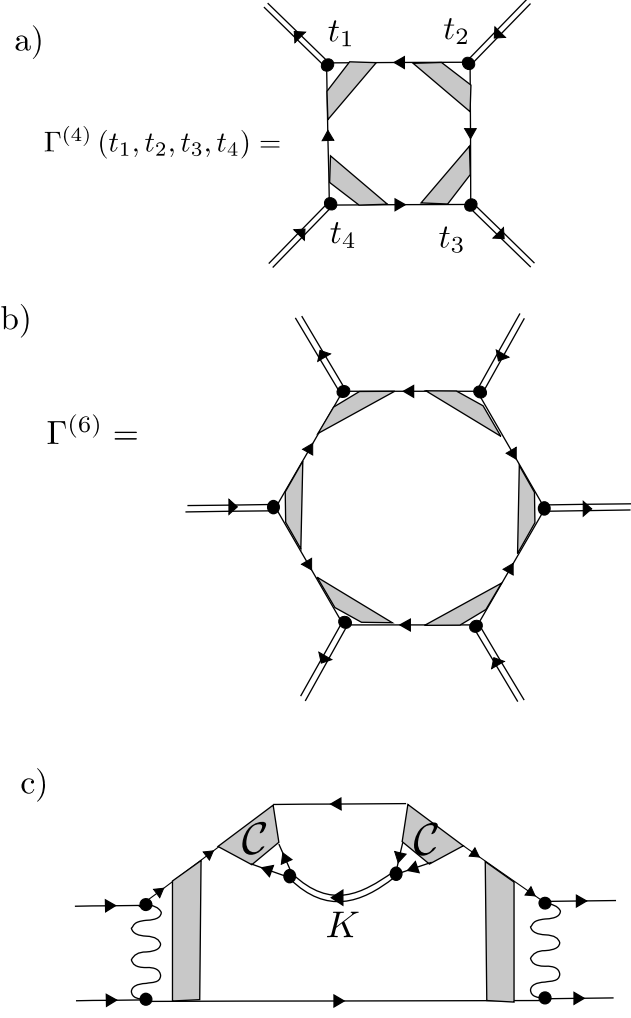


FIG. 5. a) Fermion loop with four fluctuation vertex, b) and with six. c) Contribution to  $\Pi_R$

Since this is a correction to the  $q$ -independent part of  $\Pi_R$  we may treat it as a correction to  $\epsilon(t)$ . Inserting this into the kinetic equation (10) in main text, we obtain,

$$\left[ \partial_t + \frac{16T}{\pi} (\epsilon(t) + x^2) \right] B(t, x/\xi) = T \left( 1 + a \frac{B(t, x/\xi)}{E_F \tau} \int dx' x' B(t, x'/\xi) \right), \quad (16)$$

for some  $\mathcal{O}(1)$  factor  $a$ . The additional factor is quadratic  $B$ . As the integral factor on the RHS is only weakly singular  $\sim \log \epsilon$  in equilibrium, it is sufficient to logarithmic accuracy to insist on the stated criterion  $B/E_F \tau \ll 1$ .

For example we may consider the hard quench where  $B$  is small for  $t < 0$  and then evolves under some fixed  $\epsilon = 0$  for  $t > 0$ . We first solve the equation neglecting that quadratic term, giving

$$B^0(t, x/\xi) = \frac{1 - e^{-tx^2}}{x^2}, \quad (17)$$

where we have set  $\pi/8T = 1$ . Plugging this into the quadratic term with  $q = 0$  gives  $\sim (t \log t)/E_F \tau$ . Thus the quadratic term will be a small correction as long as this is  $\ll 1$ , which to logarithmic accuracy is  $t \ll E_F \tau$ . As  $B_{q=0} = t$ , this is equivalent to the stated criterion  $B/E_F \tau \ll 1$ . Similarly, considering the quench discussed in the main text where  $\epsilon(t) = -\epsilon_f < 0$  for  $t > 0$  and  $\epsilon \sim 1$  for times  $t < 0$ , we have that

$$B^0(t, x/\xi) = \frac{1 - e^{-tx^2 + \epsilon_f t}}{x^2 + \epsilon_f}. \quad (18)$$

Inserting this into the correction term as before, we may approximate the integral over  $x'$  by noting that it is dominated by  $x' < 1/\sqrt{t}$ . Thus, the  $x'$  dependence in the denominator may be neglected if  $|\epsilon_f|t \gg 1$ . This gives that the correction term for  $q = 0$  is given by  $\exp(2\epsilon_f t)/\epsilon_f t E_F \tau$ . Insisting that this is  $\ll 1$  then gives to logarithmic accuracy the criterion stated in the text,  $t \ll \epsilon_f^{-1} \log(E_F \tau)$

## B: Equivalence to equilibrium

In equilibrium the conductivity may be equivalently expressed in terms of the Fourier transform. In equilibrium,  $B_q(t)$  is of course time independent and thus Eq. (9) and Eq. (10) imply that

$$D_R = \frac{8T}{\pi\nu} \exp \left[ -\frac{8T}{\pi} (t - t') (\epsilon + \xi^2 q^2) \right]; \quad (19)$$

$$B_q = \frac{\pi}{16} \frac{1}{\epsilon + \xi^2 q^2} \quad (20)$$

If we substitute this into the formula  $\sigma^{AL}(t, t')$ , Eq. (11 a), and Fourier transform we obtain,

$$\begin{aligned} \sigma^{AL}(\omega) &= \int_{-\infty}^{\infty} dt' e^{i\omega(t-t')} \sigma(t, t') \\ &= 32 \int dt' e^{i\omega(t-t')} \int_{-\infty}^{t'} ds \int \frac{d^2 q}{(2\pi)^2} \xi^4 q^2 \nu^2 |D_R(q, t-s)|^2 B_q \\ &= 2\pi \int dt' e^{i\omega(t-t')} \int_{-\infty}^{t'} ds \int \frac{d^2 q}{(2\pi)^2} \xi^4 q^2 \frac{\left(\frac{8T}{\pi} e^{-\frac{8T}{\pi}(t-s)(\epsilon+\xi^2 q^2)}\right)^2}{\epsilon + \xi^2 q^2} \\ &= 2\pi \int dt' e^{i\omega(t-t')} \int \frac{d^2 q}{(2\pi)^2} \xi^4 q^2 \left(\frac{8T}{\pi}\right)^2 \frac{\pi}{16T} \frac{e^{-\frac{16T}{\pi}(t-t')(\epsilon+\xi^2 q^2)}}{(\epsilon + \xi^2 q^2)^2} \\ &= 8T \int_0^{\infty} \frac{dx}{4\pi} \frac{x}{(x+\epsilon)^2} \int dt' e^{-\frac{16T}{\pi}(t-t')(-i\bar{\omega}+x+\epsilon)}; \quad \bar{\omega} \equiv \frac{\pi\omega}{16T} \\ &= \frac{1}{8} \int_0^{\infty} dx \frac{x}{(x+\epsilon)^2 (-i\bar{\omega}+x+\epsilon)} \\ &= \frac{1}{16\epsilon} \frac{2\epsilon^2}{\bar{\omega}^2} \left( -\frac{i\bar{\omega}}{\epsilon} - (1 - \frac{i\bar{\omega}}{\epsilon}) \log(1 - \frac{i\bar{\omega}}{\epsilon}) \right). \end{aligned} \quad (21)$$

Similarly for  $\sigma^{MT}$ , Eq. (11 b), we have,

$$\begin{aligned} \sigma^{MT}(\omega) &= \int_{-\infty}^{\infty} dt' e^{i\omega(t-t')} \sigma(t, t') \\ &= \int dt' e^{i\omega(t-t')} 16D \int \frac{d^2 q}{(2\pi)^2} B_q e^{-2\left(\frac{1}{\tau_{\phi}} + Dq^2\right)(t-t')} \\ &= 16D \int \frac{d^2 q}{(2\pi)^2} \frac{1}{i\omega + 2\left(\frac{1}{\tau_{\phi}} + Dq^2\right)} \frac{\pi}{16} \frac{1}{\epsilon + \xi^2 q^2} \\ &= \frac{\pi}{2} \int_0^{\infty} \frac{dx}{4\pi} \frac{1}{-i\frac{\pi\omega}{16T} + \gamma_{\phi} + x} \frac{1}{\epsilon + x}; \quad \gamma_{\phi} \equiv \frac{\pi}{8T\tau_{\phi}} \\ &= \frac{1}{8\epsilon} \left( \frac{-i\bar{\omega} + \gamma_{\phi}}{\epsilon} - 1 \right)^{-1} \log \left( \frac{-i\bar{\omega} + \gamma_{\phi}}{\epsilon} \right) \end{aligned} \quad (22)$$

These may be compared with the results in *e. g.* Francesca Federici and Andrei A. Varlamov Phys. Rev. B 55, 6070 (1997). This gives asymptotically in the various limits that

$$\sigma^{MT}(\bar{\omega}) + \sigma^{AL}(\bar{\omega}) = \frac{1}{16\epsilon} \begin{cases} \frac{4\epsilon}{-i\bar{\omega}} \log \frac{-i\bar{\omega}}{\epsilon} & \bar{\omega} \gg \epsilon, \gamma_{\phi} \\ 1 - 2 \log \frac{-i\bar{\omega}}{\epsilon} & \epsilon \gg \bar{\omega} \gg \gamma_{\phi} \\ \frac{2\epsilon}{-i\bar{\omega}} \log \frac{-i\bar{\omega}}{\epsilon} + \frac{2\epsilon}{\gamma_{\phi}} \log \frac{\gamma_{\phi}}{\epsilon} & \gamma_{\phi} \gg \bar{\omega} \gg \epsilon \\ 1 + 2 \frac{\epsilon}{\gamma_{\phi} - \epsilon} \log \frac{\gamma_{\phi}}{\epsilon} & \epsilon, \gamma_{\phi} \gg \bar{\omega} \end{cases}. \quad (23)$$

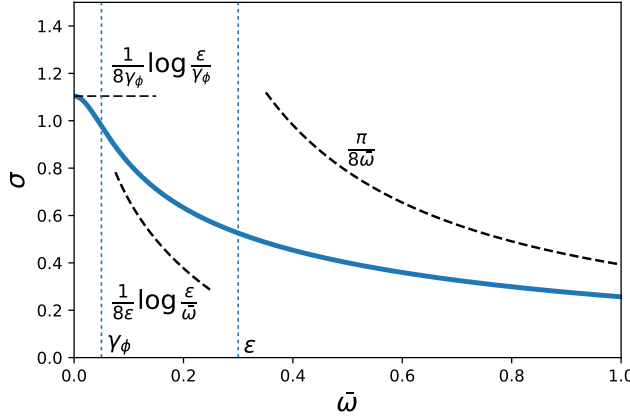


FIG. 6. Dependence of the total fluctuation conductivity  $\sigma$  on the frequency. Shown for the parameters  $\epsilon = .3$ ,  $\gamma_\phi = .05$ . Asymptotics for the different regimes are shown in dashed lines.

For example, if  $\epsilon \gg \gamma_\phi$ , we have that from  $1 \gg \bar{\omega} \gg \epsilon$  the real part of  $\sigma$  goes as  $1/|\bar{\omega}|$ . When  $\bar{\omega} \sim \epsilon$  this crosses over to a weaker logarithmic growth with  $\bar{\omega}$ , finally saturating to  $\frac{1}{8\epsilon} \log \epsilon / \gamma_\phi$  as  $\bar{\omega} \sim \gamma_\phi$ . This behavior is illustrated in Fig. 6

### C: Experimental definition of $\sigma(\omega)$

The conductivity  $\sigma(t, t')$  is defined by the relationship  $J(t) = \int dt' \sigma(t, t') E(t')$ . If delta function pulses  $E \propto \delta(t - t_0)$  could be produced, then  $J(t)$  could be measured for many such pulses and  $\sigma(t, t')$  directly reconstructed. However delta function pulses are not experimentally available.

Instead an electric field  $E(t) = f(t - t_0)$  pulse centered at  $t_0$  is applied and the induced current  $J(t)$  is (indirectly) measured. Conventionally,  $J, E$  are Fourier transformed and " $\sigma(\omega, t_0)$ " =  $J(\omega)/E(\omega)$ . These are plotted in Figs. 7, 8. We consider here the pulse shape  $f(t) = (1 - 2\frac{t^2}{w^2}) \exp(-\frac{t^2}{w^2})$ . We set  $w = 2(\pi/8T)$  although we do not find particular sensitivity to this parameter.

The primary difference between the conductivity shown here and the conductivity discussed in the main text, is that the "experimental" definition leads to highly non-monotonic behavior of the conductivity at points when the system is far from adiabaticity see Fig. 7, inset.

This wild behavior at low frequencies can be understood as follows. The Fourier transform  $E(\omega)$  goes to zero as  $\omega \rightarrow 0$  for experimentally feasible pulses. As the quantity we are considering is  $J(\omega)/E(\omega)$ , the vanishing of the denominator would be problematic. In steady state of course this is not a problem because if  $E(\omega)$  vanishes then  $J(\omega)$  must also vanish and so the ratio is finite. However, in the "experimental" calculation, when there is no time-independence, there is no reason why  $J(\omega \rightarrow 0)$  may not be finite, and thus the ratio  $J/E$  will be singular as  $\omega \rightarrow 0$ . This implies that there will be large differences between the different notions of conductivity at low frequencies when the system is farthest from adiabaticity, as observed in the overshooting behavior. This overshooting is most apparent in Fig. 7 where many solid lines over-shoot the equilibrium value (black dashed lines), with the over-shooting the largest at low frequencies.

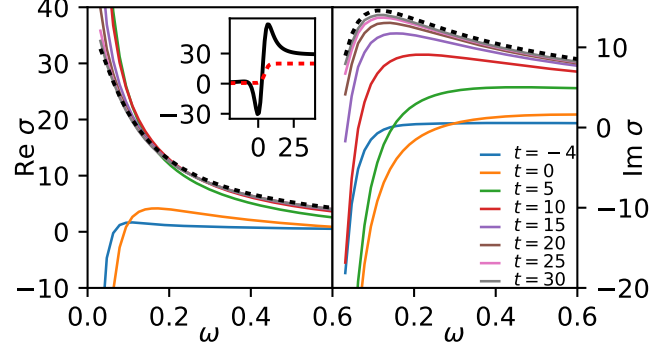


FIG. 7. The "experimental" fluctuation correction to the optical conductivity shown for several different times under the detuning given in Fig. 1 (main text), left panel. All times given in terms of  $\pi\hbar/8T$ . Inset:  $\text{Re}\sigma$  at  $\pi\omega/8T = .05$ , showing the non-monotonic behavior of the "experimental" conductivity. The red dashed line is the detuning  $\epsilon(t)$  shown at arbitrary scale.

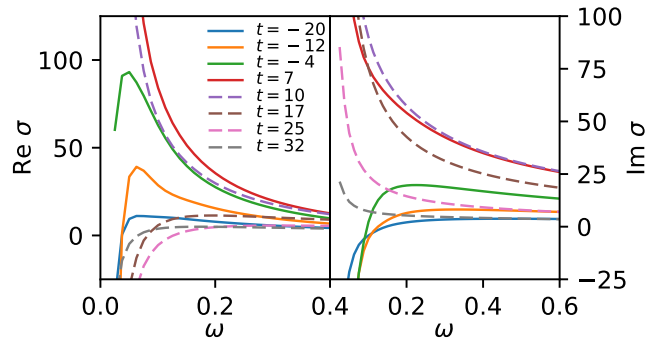


FIG. 8. The "experimental" fluctuation correction to the optical conductivity shown for several different times under the detuning given in Fig. 1 (main text), right panel. All times and inverse frequencies in units of  $\pi\hbar/8T$ .